Biochimica et Biophysica Acta 1838 (2014) 1372–1381

Contents lists available at ScienceDirect

Biochimica et Biophysica Acta

journal homepage: www.elsevier.com/locate/bbamem

# Coexistence of two liquid crystalline phases in dihydrosphingomyelin and dioleoylphosphatidylcholine binary mixtures

Masanao Kinoshita [a,b,*], Nobuaki Matsumori [a,c], Michio Murata [a,b,c,**]

[a] JST ERATO, Lipid Active Structure Project, Osaka University, 1-1 Machikaneyama, Toyonaka, Osaka 560-0043, Japan
[b] Project Research Center for Fundamental Science, Osaka University, 1-1 Machikaneyama, Toyonaka, Osaka 560-0043, Japan
[c] Department of Chemistry, Graduate School of Science, Osaka University, 1-1 Machikaneyama, Toyonaka, Osaka 560-0043, Japan

ARTICLE INFO

*Article history:*
Received 12 August 2013
Received in revised form 18 December 2013
Accepted 14 January 2014
Available online 24 January 2014

*Keywords:*
Phase diagram
Confocal fluorescence microscopy
Calorimetry
Giant unilamellar vesicle
Phase segregation

ABSTRACT

Recently, DHSM, a minor constituent in naturally occurring SMs, was indicated to form a raft-like ordered phase more effectively than a naturally occurring form of SM because DHSM has greater potential to induce the intermolecular hydrogen bond. In order to examine the influence of the DHSM-induced hydrogen bond on the phase segregation, the thermal phase behavior of stearoyl-DHSM/DOPC binary bilayers was examined using calorimetry and fluorescence observation and compared with that of SSM/DOPC binary bilayers. Results revealed that the DHSM/DOPC bilayers undergo phase segregation between two $L_\alpha$ phases within a limited compositional range. On the other hand, apparent phase separation was not observed above main transition temperature in SSM/DOPC mixtures. Our monolayer measurements showed that the lipid packing of DHSM is less perturbed than that of SSM by the addition of small amount of DOPC, indicating a stronger hydrogen bond between DHSM molecules. Therefore, in DHSM/DOPC binary bilayers, DHSM molecules may locally accumulate to form a DHSM-rich domain due to a DHSM-induced hydrogen bond. On the other hand, excess accumulation of DHSM should be prevented because the difference in the curvature between DHSM and DOPC assemblies causes elastic constraint at the domain boundary between the DHSM-rich and DOPC-rich domains. Competition between the energetic advantages provided by formation of the hydrogen bond and the energetic disadvantage conferred by elastic constraints likely results in $L_\alpha/L_\alpha$ phase separation within a limited compositional range.



## 1. Introduction

Since 1980s, it has been reported that specific domains with distinct lipid and protein compositions exist in biomembranes [1–3]. In addition, some scientists speculated that lipid distribution is not homogeneous [4] but specific lipids assemble to form distinct domains in live cells. For example, in 1982, Zalduondo et al. reported that a gel-like ordered domain exists in bovine luteal cell membranes and shows high contents of SM and chol [5]. Recently, this SM/chol-rich domain, called lipid rafts [6], has attracted scientific interest since the raft provides a platform for important biological events, including signal transduction [7–13].

The biophysical properties of the lipid rafts have been determined using model membrane systems. Previously, DSC measurements revealed that the addition of chol to SM bilayers leads to the chol-rich and chol-poor phase segregation [14] and SAXD measurements disclosed that the chol-rich domain possesses the intermediate lipid packing between the $L_\alpha$ and $L_\beta$ phases [15]. Recently, further complex systems have been employed to examine the membrane properties of rafts. For example, Veach and Keller reported that SM/chol/DOPC ternary mixtures undergo phase separation with SM/chol-rich and DOPC-rich domains [16]. FCS measurements revealed that the diffusion coefficient of the SM/chol-rich region ($0.1 \times 10^{-8}$ cm$^2$/s to $0.8 \times 10^{-8}$ cm$^2$/s) was significantly smaller than that of the DOPC-rich region (~$4.9 \times 10^{-8}$ cm$^2$/s to $5.1 \times 10^{-8}$ cm$^2$/s), but much greater than that of the $L_\beta$ (or $P_\beta$) phase in GUVs comprising pure SM, which is virtually immobile within the time scale of FCS [17]. The SM/chol-rich 'fluidizing' gel phase with an intermediate diffusion coefficient is defined as the $L_o$ phase [18] and the $L_o$ phase

*Abbreviations:* DHSM, dihydrosphingomyelin; SM, sphingomyelin; DOPC, 1,2-dioleoyl-*sn*-phosphatidylcholine; SSM, stearoyl-SM; $L_\alpha$ phase, fluid phase; chol, cholesterol; DSC, differential scanning calorimetry; SAXD, small angle x-ray diffraction; $L_\beta$ phase, gel phase; FCS, fluorescent correlation spectroscopy; $P_\beta$ phase, ripple phase; $L_o$ phase, liquid ordered phase; $L_d$ phase, liquid disordered phase; GUV, giant unilamellar vesicle; NMR, nuclear magnetic resonance; PE, phosphatidylethanolamine; bodipy-PC, 2-(4,4-difluoro-5,7-dimethyl-4-bora-3a,4a-diaza-s-indacene-3-pentanoyl)-1-hexadecanoyl-*sn*-glyceo-3-phosphocholine; $L_c$ phase, subgel phase; TR-DPPE, Texas-red dipalmitoylphosphatidylethanolamine; DEPC, 1,2-dielaidoyl-*sn*-phosphatidylcholine; DPPE, 1,2-dipalmitoyl-*sn*-phosphatidylethanolamine

* Correspondence to: M. Kinoshita, JST ERATO, Lipid Active Structure Project, Osaka University, Machikaneyama 1-1, Toyonaka, Osaka, 560-0043, Japan and Project Research Center for Fundamental Science, Osaka University, Machikaneyama 1-1, Toyonaka, Osaka, 560-0043, Japan. Tel./fax: +81 6 6850 6605.
** Correspondence to: M. Murata, JST ERATO, Lipid Active Structure Project, Osaka University, Machikaneyama 1-1, Toyonaka, Osaka, 560-0043, Japan and Project Research Center for Fundamental Science, Osaka University, Machikaneyama 1-1, Toyonaka, Osaka, 560-0043, Japan. Department of Chemistry, Graduate School of Science, Osaka University, 1-1 Machikaneyama, Toyonaka, Osaka 560-0043, Japan. Tel./fax: +81 6 6850 6605.
*E-mail addresses:* kinoshi@chem.sci.osaka-u.ac.jp (M. Kinoshita), murata@chem.sci.osaka-u.ac.jp (M. Murata).

0005-2736/$ – see front matter © 2014 Elsevier B.V. All rights reserved.
http://dx.doi.org/10.1016/j.bbamem.2014.01.017

is thought to physicochemically resemble the lipid raft because the $L_o$ domain shows strong detergent resistance, which is characteristic of lipid rafts [19–21].

Why does the SM/chol mixture conduce to the phase segregation and raft phase formation? Previously, IR spectroscopy revealed intermolecular hydrogen bond between the amide group in SM and the 3-hydroxyl group in chol [22]. Moreover, NMR spectroscopy has indicated that SM forms intramolecular and intermolecular hydrogen bonds more effectively than glycerophosphatidylcholines do [23–25]. Therefore, the electrostatic interaction between SM and chol is likely a crucial factor for the stabilization of the raft-like $L_o$ phase that phase-separated from the $L_d$ (or $L_\alpha$) phase. Despite many reports on the SM–chol hydrogen bond, contribution of the SM–SM hydrogen bond to the phase separation should be known.

In order to address this issue, some studies on miscibility of SM with unsaturated lipid have been reported. For example, Maulik et al. found that egg SM (consisting mainly of C16:0-SM) and egg PC (70% of all PCs consist of unsaturated lipids) are immiscible in fluid ($L_\alpha$) phase bilayers, whereas bovine brain SM (consisting mainly of C18:0-SM) and egg yolk PC are miscible within a certain temperature range [15]. SAXD result demonstrated that binary mixtures of egg PC and egg SM show $L_\alpha$–$L_\alpha$ immiscibility, while the mixtures of egg PC and brain SM apparently are miscible at all temperatures [26]. The MD simulations showed that phase separation occurred in SM/DOPC bilayers, which led to formation of only small clusters having cluster molecular lifetimes of less than 200 ns [27]. Anyway, so far, the subject is very complicated and, thus, influence of SM–SM hydrogen bond on the phase segregation remains unclear.

DHSM contains a saturated bond between the sphingosine C4 and C5 and accounts for 5–10% of all SMs in cultured cells, such as human skin fibroblasts and baby hamster kidney cells [28,29]. Several recent studies have indicated that the DHSM has a higher potential to provide the intermolecular hydrogen bond than the usual type of SM. For example, fluorescent quenching measurements showed that C16:0-DHSM/chol bilayers form more ordered domains than comparable C16:0-SM/chol bilayers [30]. Fluorescence microscopic observations also suggested that, in GUV consisting of C16:0-DHSM/egg PC/egg PE/chol in a 1:1:1:1 molar ratio, the $L_\beta$ phase composed of C16:0-DHSM/chol appears at room temperature, which is more ordered than the $L_o$ phase. In contrast, the replacement of C16:0-DHSM by egg-SM (mainly consisting of C16:0-SM) results in formation of the $L_o$ phase [31]. Moreover, some studies on lipid packing in pure DHSM membranes have been reported. Nyholm et al. demonstrated that a fluorescent dye, prodan, partitions less toward the $L_\alpha$ phase in the order of C16:0-DHSM > DPPC > C16:0-SM, indicating the formation of more ordered bilayers by DHSM than by SM in the absence of chol [32]. These results suggest that DHSM provide hydrogen bond more effectively than SM. Thus, it is expected that the DHSM is useful to examine the contribution of SM–SM hydrogen bond to phase separation.

The present study examined the thermal phase behavior of DHSM/DOPC binary mixtures using DSC and confocal fluorescence microscopy. Results showed that DHSM/DOPC binary bilayers experience $L_\alpha$/$L_\alpha$ phase separation within a limited compositional range at temperatures greater than the main transition temperature. Very few studies about the phase segregation between two $L_\alpha$ phases in binary phospholipid systems have been reported [33,34]; therefore, this raft-mimicking mixture that experiences phase segregation in the $L_\alpha$ phase is very interesting. In addition, a possible mechanism is proposed for the $L_\alpha$/$L_\alpha$ phase separation in the DHSM/DOPC binary mixture.

## 2. Materials and methods

### 2.1. Materials

Porcine brain SM and DOPC were purchased from Avanti Polar Lipid (Alabaster AL), and SSM was extracted from brain SM using HPLC. DHSM was prepared from SSM by hydrogenation of SSM using palladium (Wako Pure Chemical Industries, Ltd., Osaka, Japan) as a catalyst [35]. The purity of DHSM and SSM was checked by thin layer chromatography (TLC), and showing a single spot. These SMs and DOPC were separately dissolved in chloroform/methanol (4:1 v/v) at a concentration of 1 mg/mL or 10 mg/mL and stored at −20 °C until use. A fluorescent probe, bodipy-PC, was purchased from Molecular Probe (Eugene, OR). This probe was dissolved in chloroform/methanol (4:1 v/v) at a concentration of 50 μg/mL and stored in the dark at −20 °C until use.

### 2.2. DSC

The phase behavior of SM/DOPC bilayers was examined by nano-differential scanning calorimeter (Calorimetry Science Corp., UT). Bilayer samples were prepared by a conventional method. Briefly, appropriate amounts of SM and DOPC dissolved in chloroform/methanol (4:1) were mixed in a glass vial. The solution was dried under a flow of nitrogen and then under reduced pressure for at least 24 h. The resulting lipid film was dispersed into distilled and deionized water (Simplicity UV, MerckMillipore, Billerica, MA) and incubated for approximately 30 min at 55 °C for SSM mixtures and at 65 °C for DHSM mixtures with intermittent vortexing. The final concentration of SM was 5.48 mM. Then, 330 μL of the sample were placed into the DSC immediately before measurements. A scanning rate of 0.5 °C/min was used for all DSC measurements.

### 2.3. Surface pressure vs. molecular area measurements and preparation of glass-supported monolayers

Monolayers of lipid mixtures were prepared on a computer-controlled Langmuir film balance (USI System, Fukuoka, Japan) calibrated using stearic acid (Sigma Aldrich, St. Louis, MO). The subphase, which consisted of distilled, freshly deionized water, was obtained using a Milli-Q System. The apparatus was covered with vinyl sheets, which prevented deposition of dust on the water surface. The sample solution was prepared by mixing the appropriate amount of SM and DOPC solution in a micro-vial. A total of 30 μL of lipid solution (1 mg/mL) was spread onto the aqueous subphase ($100 \times 290$ mm$^2$) using a glass micropipette (Drummond Scientific Company, Pennsylvania, USA). After an initial delay period of 10 min for evaporation of the organic solvents, the monolayers were compressed at a rate of 20 mm$^2$/s. The subphase temperature and the ambient temperature were controlled to $25.0 \pm 0.1$ °C and $25 \pm 1$ °C, respectively. The measurements were repeated 3 to 5 times under the same conditions to obtain reliable results. These measurements provided the molecular area at a corresponding pressure within an error of $\sim \pm 1$ Å$^2$. The influence of oxidation on the unsaturated chains in SSM and DOPC at the air–water interface was checked by intentionally exposing pure SSM and pure DOPC monolayers to air for 10–30 min before compression [36]. The change in the isotherm after prolonged exposure of SSM or DOPC monolayers to air was within the error described above.

For the preparation of the glass-supported monolayers, the bodipy-PC (0.1–0.2 mol% of total lipids) was added to the sample solution for subsequent fluorescent microscopic observations. The micro cover glass (thickness no. 1, Matsunami, Osaka, Japan) was dipped vertically into the water followed by compression of the sample at 20 mm$^2$/s to reach the appropriate surface pressure. After compression, the glass substrate was extracted from the water at a rate of 0.2 mm/s to form the glass-supported monolayer. The fluorescence observations were conducted immediately after the sample preparation using confocal laser scanning microscopy (FV1000-D IX81, Olympus Corp., Tokyo, Japan).

### 2.4. GUV preparation and fluorescence observations

GUVs composed of SM and DOPC were prepared using the electroformation method originally developed by Angelova and Dimitrov [37]. Briefly, 5–10 μL of SM/DOPC (1:1 mol/mol) mixed solution (1 mg/mL) in the presence of 0.2 mol% bodipy-PC were spread on the surface of the electrodes, which were platinum wires (100 μm diameter), and dried under vacuum for at least 18 h. The electrode surface was coated by the thin lipid film. Then, parallel aligned electrodes were put into ~400 μL of Milli-Q water sandwiched between two cover glasses (24 mm × 60 mm, 0.12–0.17 mm thickness) using an open-square shaped rubber spacer (1 mm thickness). This chamber was fixed on a temperature-controlled sample stage (Thermo plate, Tokai hit, Shizuoka, Japan) for the subsequent microscopic observations. The DHSM/DOPC and the SSM/DOPC samples were incubated at 65 °C and 55 °C, respectively, for 30–40 min, and a low-frequency alternating current (AC) (sinusoidal wave function, 10 Vpp, 10 Hz) was applied by a function generator (20 MHz function/arbitrary waveform function generator, Agilent, Santa Clara CA). After sample preparation, the GUVs were cooled to 20 °C, equilibrated for 15 min, and then heated to the selected temperature. A scanning rate of 2 °C/min was used for the temperature-resolved observations unless otherwise mentioned. The temperature of the bulk solution was measured separately using a K-type thermometer (AD-5602A, Sansyo Industries, Ltd., Tokyo, Japan), and the temperature difference was calibrated. Fluorescence observations were conducted using confocal laser-scanning microscopy (FV1000-D IX81, Olympus Corp., Tokyo, Japan) with an air objective lens with a long working distance (LUCPLFLN 60×, Olympus Corp., Tokyo, Japan). A wavelength of 473 ± 2 nm was used for excitation of the bodipy. A laser scanning rate of 4.0 μs/pix or 8.0 μs/pix was used for the acquisition of confocal images (512 pix × 512 pix). In order to provide the clearer images for the phase separation, brightness and contrast were edited by Adobe Photo Shop CS6 (Adobe Systems Inc., CA).

## 3. Results

### 3.1. Thermal phase behavior of DHSM/DOPC and SSM/DOPC binary bilayers

Composition-dependent thermal phase behavior of DHSM/DOPC bilayers was examined using DSC and the results were compared to that of SSM/DOPC bilayers. Fig. 1a shows the DSC heating and cooling thermograms of DHSM/DOPC bilayers. In the heating thermograms, pure DHSM bilayers produced some endothermic peaks: $L_\beta$-to-$P_\beta$ phase transition (pretransition) and $P_\beta$-to-$L_\alpha$ phase transition (main transition) centered at 44.9 °C, and 52.0 °C, respectively. In addition, a broad peak centered at 32.0 ºC corresponds to the $L_c$-to-$L_\beta$ phase transition (subtransition) because prolonged low-temperature incubation enhanced its transition enthalpy (see Fig. S1). In both the heating and cooling scans, the addition of DOPC resulted in broadening of the main transition peaks, indicating that DOPC facilitates the $L_\beta/L_\alpha$ coexistent region. In the cooling thermograms of DHSM/DOPC ($x_{DOPC} = 0.3$) bilayers, a small exothermic peak newly appeared at the immediate higher temperature side of the main transition peak (indicated by an arrow in Fig. 1a), suggesting that two $L_\alpha$ phases coexisted immediately above the main transition temperature; this small peak corresponds to the phase transition between $L_\alpha$ phases. In addition, DHSM/DOPC ($x_{DOPC} = 0.4$) bilayers also provided the small exothermic peak above the main transition temperature but DHSM/DOPC ($x_{DOPC} = 0.5$) bilayers gave no indication of the $L_\alpha/L_\alpha$ phase transition (Fig. S2). Fig. 1b shows the DSC thermograms of SSM/DOPC bilayers. In the heating thermograms, pure SSM bilayers showed two endothermic peaks: the pre-transition and main transition at 32.5 °C and 44.5 °C, respectively. These results are similar to previous results [38–40]. The DSC thermograms of SSM/DOPC bilayers did not contain a peak indicating $L_\alpha/L_\alpha$ phase separation in the experimental compositional range. However, because transition enthalpy between the $L_\alpha$ phases was small and unclear, the phase behavior was examined at a higher temperature region using fluorescent microscopic observations.

### 3.2. Two $L_\alpha$ phases coexisting in DHSM/DOPC binary bilayers as shown by phase diagram

Fig. 2a shows confocal fluorescence micrographs of the DHSM/DOPC ($x_{DOPC} = 0.3$) GUVs containing 0.2 mol% bodipy-PC, which is widely used as a marker for disordered domains [41–43]. Darker domains surrounded by brighter areas were observed on the GUV surface at 43 °C. The DSC measurements indicating $L_\beta/L_\alpha$ phase separation at this temperature (see Fig. 1a) mean that the brighter and darker domains correspond to the $L_\alpha$ and $L_\beta$ phases, respectively. Coexistence of the darker and brighter domains was observed up to 62 ± 1 °C, which is significantly higher than the upper limit temperature of the main transition (Fig. 1a). This result demonstrates that DHSM-rich and DOPC-rich $L_\alpha$ phases coexist above the main transition temperature. For the coexistence of two $L_\alpha$ phases, the DHSM-rich darker domain is referred to as the $L_{\alpha1}$ phase and the DOPC-rich brighter domain as the $L_{\alpha2}$ phase (see next section for the difference in lipid packing between the DHSM-rich and DOPC-rich phases). Further increase in the temperature results in the disappearance of the darker domains and all domains transformed into the homogeneous $L_\alpha$ phase at 63 °C. Here, the stability of the $L_\alpha$ phases was checked by the incubation of the sample above the main transition temperature (Fig. 3Sa) and the $L_{\alpha1}/L_{\alpha2}$ phase separation was observed even after sample incubation at 60 °C for 15 min, suggesting that the $L_{\alpha1}$ phase, together with the $L_{\alpha2}$ phase, was stably formed above the main transition temperature. In addition, this $L_\alpha/L_\alpha$ phase segregation was also observed with another representative fluorescent probe; TR-DPPE, which was localized preferentially in the disordered phase, similar to bodipy-PC (Fig. S3b). Furthermore, the DHSM/DOPC ($x_{DOPC} = 0.45$) GUVs clearly demonstrated the appearance of $L_{\alpha1}/L_{\alpha2}$ coexistence regions far above the main transition temperature; the phase separation was maintained up to 68 ± 2 °C (Fig. 2b).

Fig. 2c shows the confocal fluorescence micrographs of SSM/DOPC ($x_{DOPC} = 0.3$) binary GUVs containing 0.2 mol% bodipy-PC. A darker region surrounded by a brighter region was observed at 41 °C. DSC measurements showed the coexistence of the $L_\beta$ and $L_\alpha$ phases under these conditions (Fig. 1b). This phase separation nearly disappeared at 49 °C (Fig. 2c), which is close to the upper temperature limit of the main transition (Fig. 1b). Thus, an SSM/DOPC ($x_{DOPC} = 0.3$) bilayer is likely to form a homogeneous $L_\alpha$ phase above the main transition temperature. In addition, the phase separation disappeared at 45 °C in SSM/DOPC ($x_{DOPC} = 0.5$) bilayers (Fig. 2d).

According to the DSC results and confocal fluorescence observations, the phase diagrams for DHSM/DOPC and SSM/DOPC binary bilayers were suggested in Fig. 3. DHSM/DOPC bilayers gave rise to segregation of the $L_{\alpha1}$ and $L_{\alpha2}$ phases within a limited compositional range. In contrast, the phase boundary in the higher temperature region of SSM/DOPC mixtures decreased with an increase in DOPC composition. Thus, coexistence of two $L_\alpha$ phases is unlikely above their main transition temperatures, according to the phase rule. This result for SSM/DOPC mixture could be supported by previous reports; egg PC (70% of all PCs consist of unsaturated lipids) and brain SM (~50% of all SM consist of SSM) are miscible in the $L_\alpha$ phase [15,41]. In addition, similar confocal fluorescence observations demonstrated that C16:0-SM/DOPC bilayers showed the coexistence of $L_\beta/L_\alpha$ phases, but no further phase separation [42].

### 3.3. Difference in lipid packing in DHSM/DOPC and SSM/DOPC binary mixtures

To obtain information on the lipid packing in DHSM/DOPC and SSM/DOPC mixtures, surface pressure vs. molecular area isotherm ($\pi$-$A$ isotherm) measurements using the monolayer systems were conducted. Fig. 4a shows the $\pi$-$A$ isotherms of DHSM/DOPC binary monolayers at

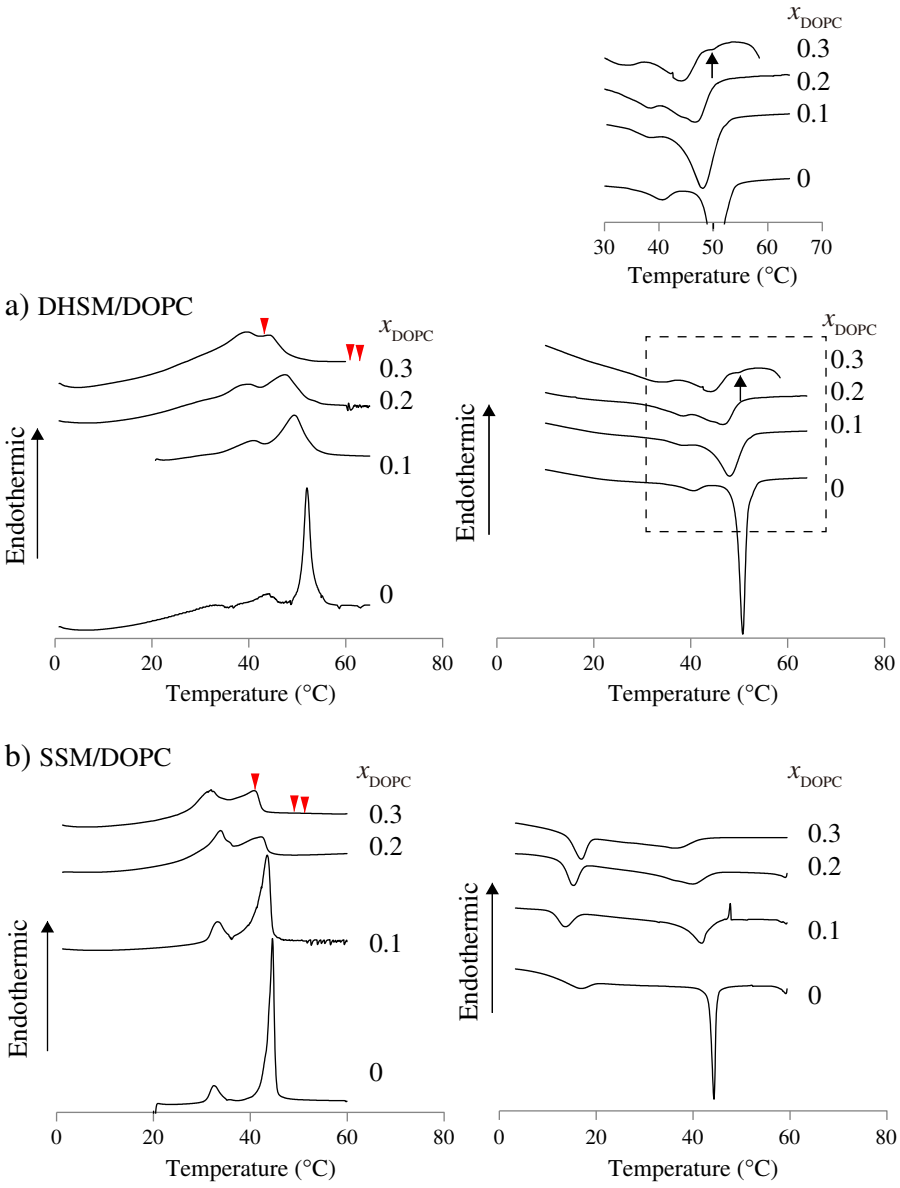


**Fig. 1.** DSC thermograms of (a) DHSM/DOPC bilayers (b) SSM/DOPC bilayers. The left and right panels correspond to the heating and cooling scans, respectively. Insertion in (a) represents magnification of the region bounded by the dashed square. The arrows indicate the exothermic peak corresponding to the phase transition between $L_\alpha$ phases. The arrowheads indicate the temperatures at which confocal images are shown in Fig. 2a and c. The molar fraction of DOPC $x_{DOPC}$ is described directly. Evaporation of gas dissolved in the water occurred in the higher temperature region.

25 °C. The pure DHSM monolayer showed a liquid-expanded (LE) to liquid-condensed (LC) phase transition at 2–5 mN/m and collapsed at 73.2 mN/m. Similar phase behavior also was observed in the monolayer of a DHSM/DOPC ($x_{DOPC} = 0.1$) binary mixture. In contrast, DHSM monolayers in the presence of 30 mol% and 50 mol% DOPC experienced a step-wise collapse at 50.5 ± 0.5 mN/m and 67.5 ± 0.5 mN/m. Previously, *π-A* isotherm measurements and atomic force microscopic observations revealed that a monolayer composed of ordered and disordered phases showed a step-wise collapse, with the latter domain becoming selectively squeezed out immediately above the first collapse pressure [43]. Thus, in the present study, two phases should coexist in DHSM/DOPC monolayers at these compositions, and the DOPC-rich disordered domain first collapsed in the lower pressure region. A further increase in the concentration of DOPC resulted in a single collapse at ~48 ± 1 mN/m.

To discuss the composition dependence of the phase behavior, collapse pressure was plotted as a function of $x_{DOPC}$ (Fig. 4b). At lower DOPC concentrations ($0 \le x_{DOPC} \le 0.15$–$0.2$), the collapse pressure of DHSM/DOPC binary monolayers monotonously decreased as DOPC concentration increased, indicating that DHSM and DOPC are miscible and form a homogeneous monolayer. A further increase in DOPC concentration ($0.15$–$0.2 \le x_{DOPC} \le 0.6$–$0.7$) produced step-wise collapse, indicating the coexistence of DHSM-rich and DOPC-rich domains. Because the greater collapse pressure of 66.2 ± 1.8 mN/m is close to the collapse pressure of DHSM/DOPC at $x_{DOPC} = 0.15$ (65.1 mN/m), and the lower collapse pressure at 49.3 ± 1.3 mN/m is close to that of DHSM/DOPC at $x_{DOPC} = 0.7$ (48.9 mN/m), DHSM/DOPC ($x_{DOPC} = 0.15$–$0.2$) and DHSM/DOPC ($x_{DOPC} = 0.6$–$0.7$) are likely to coexist within the intermediate compositional range. At higher concentrations of DOPC ($0.6$–$0.7 \le x_{DOPC} \le 1$), the step-wise collapse was not observed. Thus, DHSM and DOPC are considered miscible under these conditions. These results agree with fluorescence observations of their glass-supported monolayers immediately below the first collapse pressure. The fluorescent image of DHSM/DOPC ($x_{DOPC} = 0.5$) showed darker regions surrounded by the brighter matrix (Fig. 4c). Considering that the bodipy-PC preferentially localizes in the disordered phase, the darker domain corresponds to

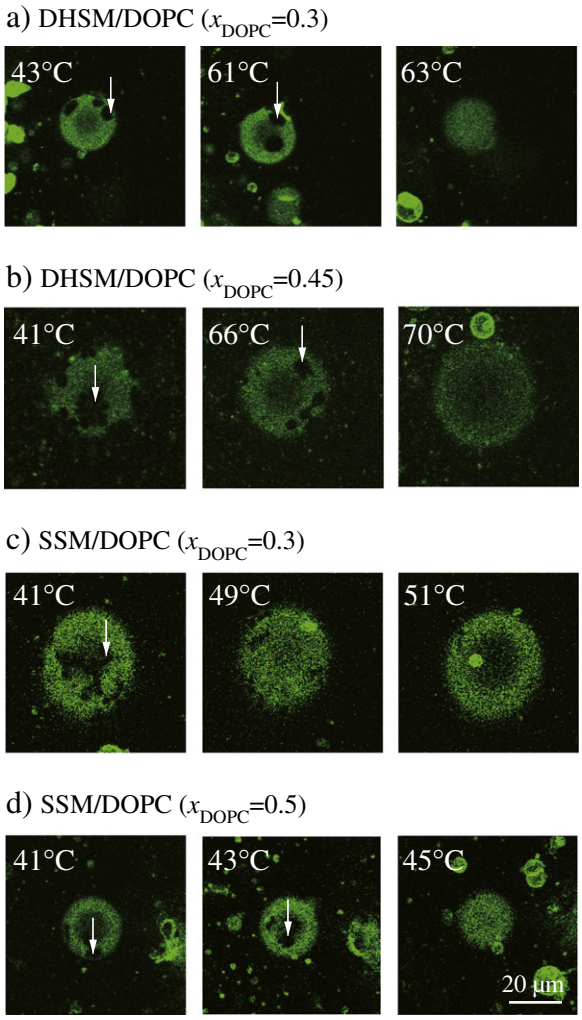


**Fig. 2.** Confocal fluorescence micrographs of (a, b) DHSM/DOPC and (c, d) SSM/DOPC binary GUVs in the presence of the 0.2 mol% bodipy-PC, respectively. The brighter region corresponds to the DOPC-rich disordered domain and the darker region corresponds to the DHSM-rich ordered domain (indicated by arrows).

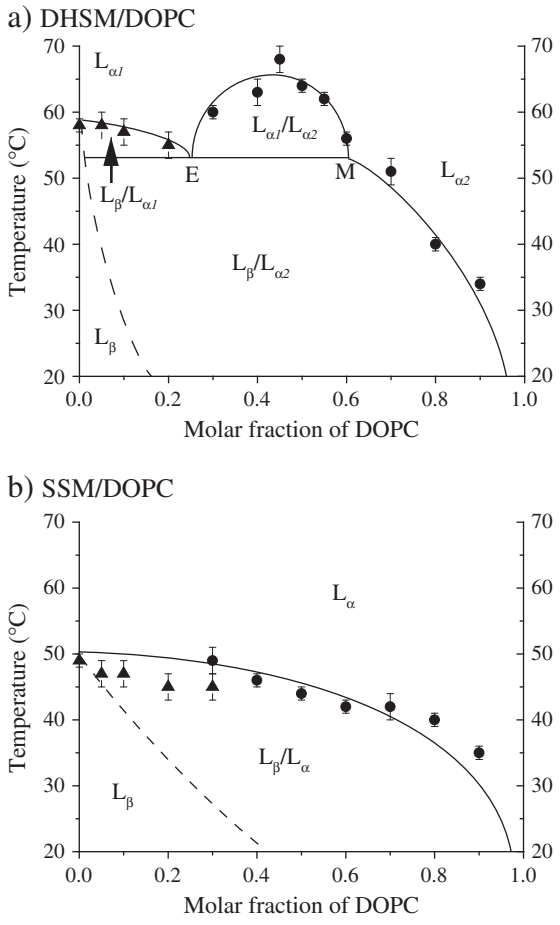


**Fig. 3.** Phase diagrams of (a) DHSM/DOPC and (b) SSM/DOPC binary bilayers. Phase boundaries at lower DOPC concentrations were estimated from DSC thermograms; triangles correspond to the upper limit temperature of the main transition of mixtures because the end-temperature of the main transition in the DSC heating thermogram corresponds to the disappearance temperature of the darker domain in the fluorescent observations. The phase boundary at higher DOPC concentrations was estimated from confocal fluorescence observations; circles correspond to the temperature at which the darker region disappeared. The phase boundary between the homogeneous $L_\beta$ phase region and the $L_\beta/L_\alpha$ phase coexistence region (dashed lines) could not be determined accurately because the superposition of the pre-transition peak on the main transition obscures the lower temperature limit of the main transition. The other phase boundaries were determined by the phase rule.

the DHSM-rich ordered phase and the brighter matrix corresponds to the DOPC-rich disordered phase. In addition, the areal ratio of DHSM-rich darker domain from three randomly selected micrographs of the DHSM/DOPC ($x_{DOPC} = 0.5$) monolayer was measured and revealed that 15 ± 5% of all domains transform into the DHSM-rich domain under these conditions. In contrast, the fluorescence images of DHSM/DOPC ($x_{DOPC} = 0.1$) and DHSM/DOPC ($x_{DOPC} = 0.9$) monolayers did not show a phase separation.

Furthermore, to compare the lipid packing characteristics of the DHSM-rich and DOPC-rich phases, the mean molecular area $A_{mes}$ was plotted as a function of $x_{DOPC}$ at 30 mN/m, which is immediately below the first collapse pressure (Fig. 4d). At lower DOPC concentrations ($0 \le x_{DOPC} \le 0.15$–$0.2$), the $A_{mes}$-values nearly corresponded to the additivity line. Together with the fluorescence observations and the collapse pressure analysis (Fig. 4b and c), these results indicate that the DHSM and DOPC, at $x_{DOPC} \le 0.15$–$0.2$, are miscible without perturbation of the lipid packing. At $0.15$–$0.2 \le x_{DOPC} \le 0.6$–$0.7$, the $A_{mes}$ value increased linearly as the $x_{DOPC}$ increased, deviating positively from the additivity lines. Thus, under these conditions, the DHSM-rich phase coexists with the DOPC-rich phase, where the lipid packing of DHSM must be perturbed by DOPC. At higher concentrations of DOPC ($x_{DOPC} > 0.6$–$0.7$), the $A_{mes}$ values were nearly constant, irrespective of the composition, and were similar to the lateral occupied area of the pure DOPC molecule (62 Å$^2$). Thus, under these conditions, DHSM molecules adopt a lateral occupation area similar to that of DOPC because of the perturbation of the lipid packing. Use of the composition of the DHSM- and DOPC-rich domains in addition to the apparent partial molecular areas of DHSM and DOPC in each domain, the areal ratio of the DHSM-rich domain to all monolayer domains in the DHSM/DOPC ($x_{DOPC} = 0.5$) monolayer was calculated to be 24 ± 8% (see appendix for calculation). This value is consistent with that estimated directly from their confocal micrographs (15 ± 5%) within the error.

The *π-A* isotherms of SSM/DOPC binary monolayers were used as a control (Fig. 5a). Pure SSM monolayers showed the LE-to-LC phase transition at 8–14 mN/m, which is higher than that for the pure DHSM monolayer (2 mN/m–5 mN/m; Fig. 4a), indicating that the DHSM monolayer forms an ordered phase more readily compared to the SSM monolayer. The pure SSM monolayer collapsed at 58.9 mN/m. In SSM/DOPC binary monolayers, the collapse pressure decreased almost continuously as $x_{DOPC}$ increased, and a step-wise collapse was not observed (Fig. 5b). These results indicate that SSM and DOPC are miscible and form a homogenous monolayer throughout the composition range. In addition, fluorescence observations of the supported monolayers also

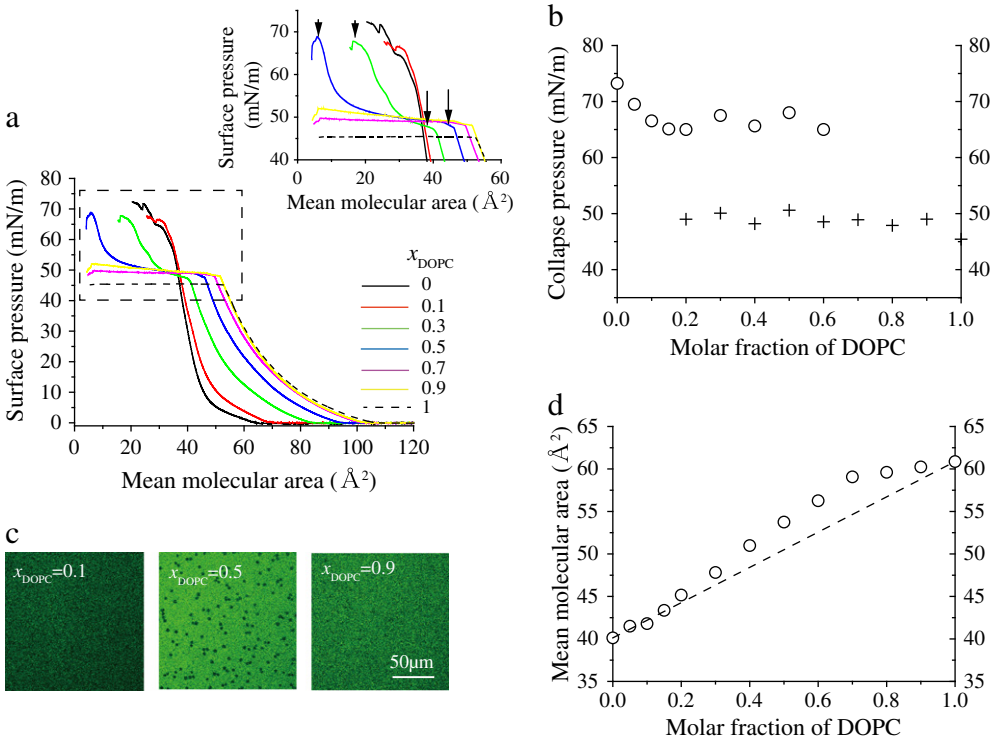


**Fig. 4.** (a) Surface pressure vs. molecular area isotherms of DHSM/DOPC monolayers. Insertion in (a) represents magnification of the region bounded by the dashed square. Several isotherms were omitted from the figure for simplicity. (b) Collapse pressure vs. composition plot. Circles and crosses indicate collapse pressure of the DHSM-rich and DOPC-rich domains (see arrowheads and an arrow in (a)), respectively. (c) Confocal fluorescent micrographs of DHSM/DOPC supported monolayers at 30 mN/m. (d) Mean molecular area ($A_{mean}$) vs. composition plot at 30 mN/m. The $A_{mean}$ values were estimated from the $\pi$-$A$ isotherms shown in (a). The additivity function is indicated by the dashed line.

showed no phase separation (Fig. 5c). The lipid packing features of the SSM/DOPC monolayer were determined from the $A_{mes}$ vs. composition plots (Fig. 5d). The SSM/DOPC ($x_{DOPC} = 0.1$) monolayer produced $A_{mes}$ values larger than the additivity value, suggesting that the packing of SSM molecules was easily perturbed, even in the presence of a small amount of DOPC.

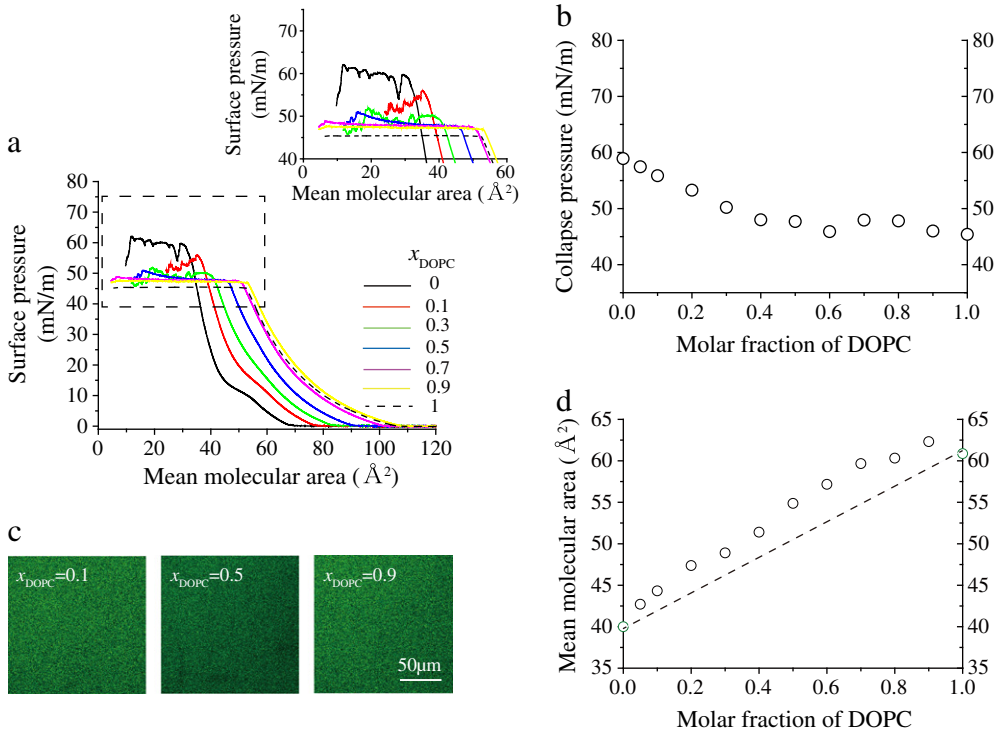


**Fig. 5.** (a) Surface pressure vs. molecular area isotherms of SSM/DOPC monolayers. Insertion in (a) represents magnification of the region bounded by the dashed square. Several isotherms were omitted from the figure for simplicity. (b) Collapse pressure vs. composition plot. (c) Confocal fluorescence micrographs of SSM/DOPC supported monolayers at 30 mN/m. (d) Mean molecular area ($A_{mean}$) vs. composition plot at 30 mN/m. The $A_{mean}$ values were estimated from $\pi$-$A$ isotherms shown in (a). The additivity function was indicated by the dashed line.

### 3.4. Miscibility between DHSM and SSM mixtures

It is important to determine whether DHSM stabilizes the raft together with usual SM or whether it separately forms a DHSM-rich raft in biomembranes. Therefore, the miscibility between DHSM and SSM was examined using monolayer measurements. Fig. 6a shows the *π-A* isotherms of DHSM/SSM binary monolayers at 25 °C. Based on the *π-A* isotherms, the collapse pressure was plotted as a function of the molar fraction of SSM $x_{SSM}$ (Fig. 6b). Step-wise collapse of the monolayer was observed up to $x_{SSM} = 0.6–0.7$, although the isotherm of DHSM/SSM at $x_{SSM} = 0.7$ did not clearly show a step-wise collapse (Fig. 6a). Because the collapse pressure of pure SSM monolayer (58.9 mN/m) was lower than that of pure DHSM monolayer (73.2 mN/m), the SSM-rich domain collapsed at a lower pressure region (~63.4 mN/m), followed by the collapse of the DHSM-rich domain (~72.6 mN/m). In addition, the DHSM-rich domain appears to consist of nearly pure DHSM while the SSM-rich domain consists of a mixture of DHSM and SSM ($x_{SSM} = 0.6–0.7$) because the collapse pressures are similar to those of the pure DHSM and DHSM/SSM ($x_{SSM} = 0.6–0.7$) monolayers (62.3 mN/m), respectively. A further increase in SSM concentration ($x_{SSM} \geq 0.6–0.7$) resulted in monotonous collapse of the monolayer, indicating homogeneous membrane formation. A previous report stated that DHSM is a minor component, accounting for 5–10% of all SMs in cultured cell membranes [28,29]. Thus, our results suggest that DHSM and SSM are miscible in those membranes.

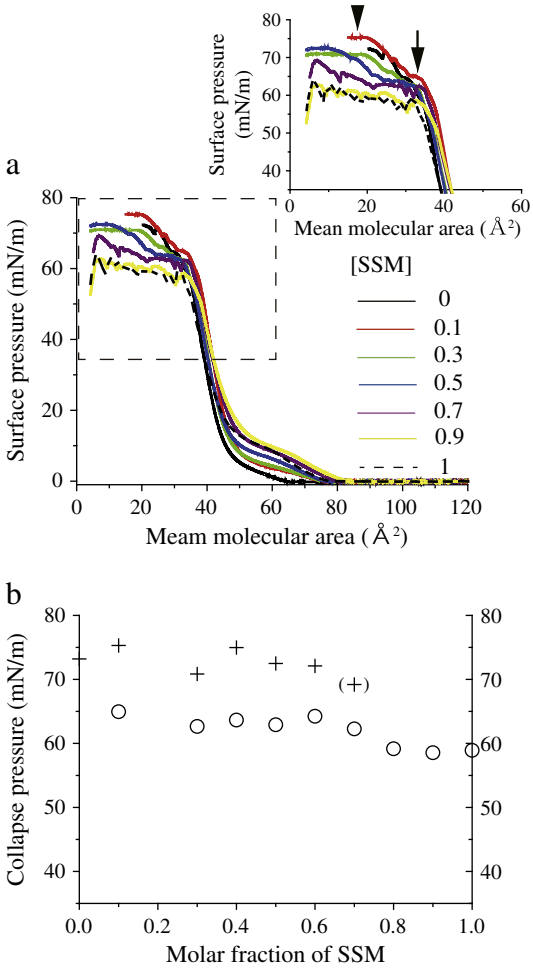


**Fig. 6.** (a) Surface pressure vs. molecular area isotherms of DHSM/SSM monolayers. Several isotherms were omitted from the figure for simplicity. Insertion in (a) represents magnification of the region bounded by the dashed square. The first and second collapses are indicated by the arrowhead and arrow, respectively, in the thermogram of the DHSM/SSM mixture at $x_{SSM} = 0.1$ (b) Collapse pressure vs. composition plot. Crosses indicate the collapse pressure of the DHSM-rich domain and circles indicate the collapse pressure of the SSM-rich domain.

## 4. Discussion

### 4.1. $L_\alpha/L_\alpha$ phase separation in DHSM/DOPC binary bilayers

The DHSM has greater potential to induce intermolecular hydrogen bonds compared to SM, not only in the gel phase but also in the $L_\alpha$ phase [25,32]. This probably explains why DHSM shows greater affinity to chol than SSM does, and thus a DHSM/chol mixture forms a more ordered phase [22,28,30,31,44,45]. However, no information on the miscibility in DHSM/unsaturated lipid binary systems is available. In the present study, we aimed to disclose the intrinsic potential of DHSM for the phase segregation in the absence of chol.

In DSC cooling thermograms, DHSM/DOPC ($x_{DOPC} = 0.3$ and 0.4) bilayers showed a small exothermic peak at the higher temperature side of the main transition (Figs. 1a and S2b), suggesting the coexistence of two $L_\alpha$ phases immediately above the main transition temperature. On the other hand, DHSM/DOPC bilayers at $x_{DOPC} = 0.5$ gave no indication of the phase transition (Fig. S2a). This behavior is in line with previous report [34]; the transition enthalpy between the $L_{\alpha1}$ and $L_{\alpha2}$ phases became small in the vicinity of the point M in their phase diagram (see Fig. 3a). In addition, no peaks corresponding to the phase transition between the $L_\alpha$ phases were seen in the heating thermograms of the same mixtures (Fig. 1a). In general, an endothermic peak in DSC heating scans has a long tail toward the higher temperature region because of the relaxation process. Thus, the long tail of the main transition peak may obscure the small peak at the higher temperature side of the main transition. For further comparison between the DSC thermogram and phase diagram, additional experiments such as X-ray diffraction and spectroscopic methods are necessary to determine the precise phase boundary of the $L_{\alpha1}/L_{\alpha2}$ coexistence region.

The phase behavior of DHSM bilayers at higher DOPC concentrations ($x_{DOPC} \geq 0.3$) was examined using fluorescence observations. In DHSM/DOPC ($x_{DOPC} = 0.45$) GUVs, confocal microscopy revealed the coexistence of DHSM-rich ($L_{\alpha1}$) and DOPC-rich ($L_{\alpha2}$) phases above the main transition temperature (Fig. 2b). A previous report indicated that DEPC/DPPE binary bilayers demonstrated coexistence of the two $L_\alpha$ phases and the phase diagram of this mixture was similar to that of DHSM/DOPC mixtures [33]. Considering that diacyl-PE induces strong hydrogen bonds [46,47], the intermolecular hydrogen bond may be an important factor in the induction of the $L_\alpha/L_\alpha$ phase separation, although the previous report have suggested a different mechanism for $L_\alpha/L_\alpha$ phase segregation in DEPC/DPPE mixtures.

Fluorescence observation of membranes has some inherent problems. For example, acceleration of the photo-oxidation of unsaturated lipids is most noticeable near the miscibility transition and increases the transition temperature, leading to the formation of smaller domains in vesicles [16,48,49]. In addition, these effects depend on the degree of unsaturation of acyl chains [50]. Thus, we examined influence of the photo-oxidation on the thermal phase behavior using a GUV comprising of DHSM and POPC, which was substituted with one unsaturated acyl chain in comparison with DOPC bearing double unsaturated acyl chains. Our preliminary measurements showed that DHSM/POPC bilayers also undergo the phase segregation above main transition temperature as in the case for the DHSM/DOPC bilayer (Fig. S4). These results support that the $L_\alpha/L_\alpha$ phase segregation observed in DHSM/DOPC GUVs is not an artifact coming from the photo-oxidation.

Lipid packing in the $L_{\alpha1}$ and $L_{\alpha2}$ phases was estimated using surface pressure vs. molecular area isotherm measurements (Fig. 4d). The lipid packing of DHSM was found to be less perturbed than SSM by the addition of a small amount of DOPC ($x_{DOPC} \leq 0.15–0.2$) probably because of relatively strong hydrogen bond between DHSM molecules. On the other hand, the $A_{mean}$ values were significantly larger than the additivity line in the range of $x_{DOPC} \geq 0.6–0.7$, indicating the packing of DHSM was

perturbed under the higher concentration of DOPC. In addition, similar $x_{DOPC}$-dependence of $A_{mes}$ was observed at other surface pressures (Fig. S5). It is expected that the lipid packing in the $x_{DOPC} \leq 0.15$–$0.2$ and $x_{DOPC} \geq 0.6$–$0.7$regions observed in the monolayer systems could correspond to those of the $L_{\alpha 1}$ and $L_{\alpha 2}$ phases in the bilayer systems, respectively. In contrast, the SSM/DOPC ($x_{DOPC} = 0.1$) monolayer produced larger $A_{mes}$ values compared to the additivity even in the lower composition of DOPC (Fig. 5d), suggesting that the packing of SSM molecules is easily perturbed in the presence of a small amount of DOPC ($x_{DOPC} \leq 0.1$). Because SSM has a lower capacity for forming intermolecular hydrogen bonds compared to DHSM, these results seem reasonable.

### 4.2. Mechanism for $L_o/L_\alpha$ phase separation in DHSM/DOPC binary bilayers

In order to determine the mechanism for the compositional-dependence phase behavior observed in this study; $L_{\alpha 2} \rightarrow L_{\alpha 2}/L_{\alpha 1} \rightarrow L_{\alpha 1}$, assumptions included: (1) DHSM assembly produces stronger hydrogen bond than SSM, and (2) DHSM assembly tends to form a vesicle smaller than the DOPC assembly does. The first assumption is based on the areal analysis (Fig. 4d) and previous reports [25,32]. The second assumption is supported by DLS experiments; DHSM assembly in the $L_\alpha$ phase formed vesicles with the average particle size of 1.2 μm, which is significantly smaller than that of DOPC assembly with the average particle size of 3.2 μm (Fig. S6). Under the higher concentration of DOPC ($x_{DOPC} \geq x_2$), DHSM and DOPC are miscible, leading to a homogeneous $L_{\alpha 2}$ phase (Fig. 7a). Further increase in DHSM content results in the domain formation due to hydrogen bonds between DHSM molecules (assumption (1) and Fig. 7b), where the enthalpic advantage may overcome the entropic disadvantage. Then, DHSM molecules become incorporated into the DHSM-rich region to form hydrogen bonds and, consequently, DHSM-rich domains ($L_{a1}$ phase) are formed in the DOPC-rich matrix ($L_{a2}$ phase) as shown in Fig. 7c. Here, according to the lever rule, the compositions of the DHSM-rich and DOPC-rich domains are $x_{DOPC} = x_1$ and $x_{DOPC} = x_2$, respectively (Fig. 7f and c).

One of the reasons that the DHSM content in the DHSM-rich domains stays constant at $x_{DOPC} = x_1$, regardless of the total DHSM/DOPC ratio, may be the curvature difference between DHSM and DOPC assemblies, because a large difference in DHSM contents in a domain causes a curvature gap (assumption (2) and Fig. S6), possibly resulting in the discontinuity of curvature at the domain boundary (Fig. 7d). This elastic constraint at the domain boundary could prohibit a further increase in the DHSM content of the DHSM-rich domain, leading instead to the lateral proliferation of the DHSM-rich domain while keeping the composition constant at $x_{DOPC} = x_1$ (Fig. 7e). And, at higher DHSM contents in the range of $x_{DOPC} < x_1$, the homogeneous $L_{\alpha 1}$ phase occurs (Fig. 7f). To support this idea, we added chol to the DHSM/DOPC mixture at $x_1 < x_{DOPC} < x_2$ and intentionally enhanced the local concentration of DHSM; it has been reported that the addition of chol to SSM/DOPC mixtures leads to the formation of SSM-rich $L_o$ domains (compare ref. [15,41] and [17,51]) and the chol-induced SM accumulation is thought to be more favorable in DHSM/DOPC mixtures because of stronger affinity between DHSM and chol [31]. As a result, the addition of chol drove DOPC away from $L_o$ domains and caused a curvature

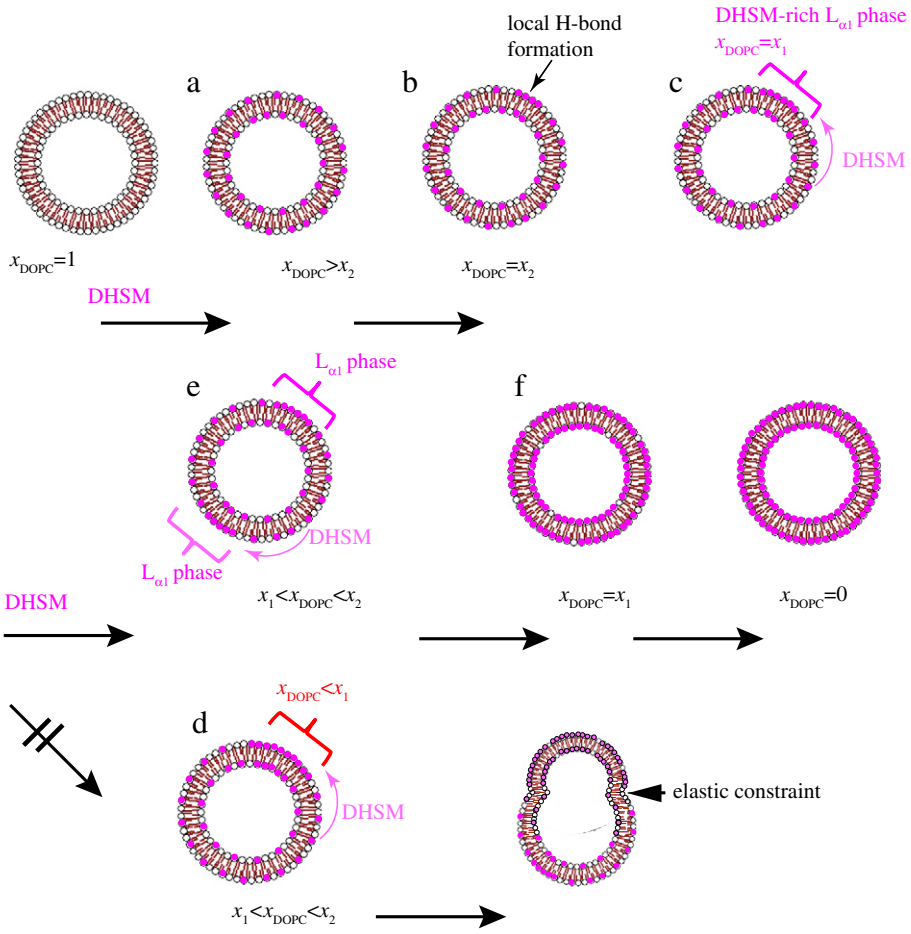


**Fig. 7.** Schematic illustrations of the mechanism for $L_o/L_\alpha$ phase separation in DHSM/DOPC binary bilayers (see Fig. 3a). The lipids with red and white headgroups show DHSM and DOPC, respectively. The $x_2$ and $x_1$ represent molar fractions of DOPC at the phase boundaries between the homogeneous-$L_{\alpha 2}$ phase and $L_{\alpha 1}/L_{\alpha 2}$ phase coexistence regions and between the $L_{\alpha 1}/L_{\alpha 2}$ phase coexistence and homogenous $L_{\alpha 1}$ phase regions, respectively.

discontinuity with $L_d$ domains [52], leading to the protrusion of a DHSM-rich ordered portion from the GUV surface (Fig. S7). In the presence of chol, the hydrogen bonds between DHSM molecules may be enhanced enough to overcome the elastic constraint caused by curvature discontinuity.

In contrast to the phase behavior of DHSM/DOPC, SSM/DOPC bilayers showed no $L_\alpha/L_\alpha$ phase separation upon the confocal microscopic observation (Fig. 2c and d). Considering the stronger intermolecular interaction of DHSM than that of SSM, the hydrogen bonding should play a key role in the $L_\alpha/L_\alpha$ phase separation.

## 5. Conclusions

DSC and confocal fluorescence microscopy showed that the DHSM/DOPC binary bilayer undergoes $L_\alpha/L_\alpha$ phase separation within a certain composition range. Although the raft-mimic $L_o/L_d$ (or $L_\alpha$) phase separation currently attracts scientific interests, the $L_\alpha/L_\alpha$ phase segregation observed in the present study revealed an intrinsic potential of the DHSM molecule for the phase segregation even in the absence of chol. In addition, our monolayer measurements showed that the lipid packing of DHSM was not perturbed under lower concentrations of DOPC (Fig. 4d), indicating strong hydrogen bond among DHSM molecules. On the basis of these results, the mechanism for $L_\alpha/L_\alpha$ phase separation is proposed as follows. When DHSM molecules are added to DOPC bilayers, DHSM starts to form a DHSM-rich complex at a certain composition probably because of its high capacity of the hydrogen bond formation. However, excess accumulation of DHSM is prevented because the difference in the curvature between DHSM and DOPC assemblies (Fig. S6) causes elastic constraint at their domain boundaries. Probably, energetic competition between (1) and (2) results in the $L_\alpha/L_\alpha$ phase separation within a limited compositional range. Finally, $\pi$-$A$ isotherm measurements revealed that DHSM and SSM are miscible at higher SSM concentrations ($x_{SSM} \geq 0.6$–$0.7$), implying that DHSM and SM are miscible in the usual cultured cell membranes, in which DHSM account for 5–10% of all SMs. Speculatively, DHSM supports rigid raft domain formation together with SM in cultured cell membranes because the presence of DHSM with a flexible saturated C4-C5 bond allows neighboring SMs to closely approach each other to enhance the intermolecular hydrogen bonding between SM and DHSM molecules, and probably also between SMs molecules.

Supplementary data to this article can be found online at http://dx.doi.org/10.1016/j.bbamem.2014.01.017.

## Acknowledgements

The hydrogenation of sphingomyelin was conducted by Dr. Sebastien Lethu (ERATO Murata Lipid Active Structure Project, Osaka University) and Mr. Yasuo Nakagawa (Murata Lab. Department of Chemistry, Graduate School of Science, Osaka University). This work was carried out by the JST-ERATO Murata Lipid Active Structure Project.

## Appendix A

On the basis of data shown in Fig. 4b and d, the areal ratio of the DHSM-rich ordered domain in DHMS/DOPC ($x_{DOPC} = 0.5$) was calculated and compared with that obtained by fluorescence observation (Fig. 4c).

The molar fractions of DOPC in the DHSM-rich (dark) and the DOPC-rich (bright) domains were defined as $x^D_{DOPC}$ and $x^B_{DOPC}$, respectively, and the total number of the molecules contained in the DHSM-rich and DOPC-rich domains are $N_D$ and $N_B$, respectively. The total amount of DHSM $N_{DHSM}$ and DOPC $N_{DOPC}$ in this system was expressed as

$$N_{DHSM} = \left(1-x^D_{DOPC}\right)N_D + \left(1-x^B_{DOPC}\right)N_B \quad (1)$$

$$N_{DOPC} = x^D_{DOPC}N_D + x^B_{DOPC}N_B \quad (2)$$

Because the amounts of DHSM and DOPC molecules in the DHSM/DOPC mixture at $x_{DOPC} = 0.5$ are equal $N_{DHSM} = N_{DOPC}()$, $N_D$ and $N_B$ can be expressed as

$$N_D = C\left(2x^B_{DOPC}-1\right) \quad (4)$$

$$N_B = C\left(1-2x^D_{DOPC}\right) \quad (5)$$

where $C$ is a proportional constant.

In addition, the partial molecular areas of DHSM and DOPC were defined in the DHSM-rich and DOPC-rich domains as $A^D_{DHSM}$ and $A^D_{DOPC}$, and $A^B_{DHSM}$ and $A^B_{DOPC}$, respectively. The areas of the DHSM-rich $A_D$ and DOPC-rich domains $A_B$ can be expressed as

$$A_D = A^D_{DHSM}N_D\left(1-x^D_{DOPC}\right) + A^D_{DOPC}N_Dx^D_{DOPC} \quad (6)$$

$$A_B = A^B_{DHSM}N_B\left(1-x^B_{DOPC}\right) + A^B_{DOPC}N_Bx^B_{DOPC} \quad (7)$$

Because the lipid packing is not perturbed by DOPC in the DHSM-rich domain, the partial molecular area of DOPC (62 Å$^2$) should be approximately 1.5-fold greater than that of DHSM (40 Å$^2$) (see Text and Fig. 4d). In contrast, in the DOPC-rich domain, the lipid packing of DHSM is perturbed and the partial molecular area of DHSM is similar to that of DOPC (62 Å$^2$).

Therefore, the areal ratio $r$ of the DHSM-rich dark domain to all domains can be estimated by

$$r = \frac{A_D}{A_D + A_B} = \frac{\left(2x^B_{DOPC}-1\right)\left(1+0.5x^D_{DOPC}\right)}{2x^B_{DOPC} + x^B_{DOPC}x^D_{DOPC} - 3.5x^D_{DOPC} + 0.5} \quad (8)$$

Because the molar fraction of $x_{DOPC}$ in the DHSM-rich and DOPC-rich domains were roughly estimated to be 0.15–0.20 and 0.60–0.73, respectively, on the basis of the data shown in Fig. 4b, the $r$-value was calculated to be $0.24 \pm 0.8$ according to Eq. (8).

## References

[1] E. Rodriguez-Boulan, W.J. Nnelson, Morphogenesis of the polarized epithelial cell phenotype, Science 245 (1989) 718–725.
[2] A.M. Craig, G. Banker, Neuronal polarity, Annu. Rev. Neurosci. 17 (1994) 267–310.
[3] J.R. Bartles, The spermatid plasma membrane comes of age, Trends Cell Biol. 5 (1995) 400–404.
[4] S.J. Singer, G.L. Nicolson, Fluid mosaic model, Science 175 (1972) 720–731.
[5] F. Goodsaid-Zalduondo, D.A. Rintoul, J.C. Carlson, W. Hansel, Luteolysis-induced changes in phase composition and fluidity of bovine luteal cell membranes, Proc. Natl. Acad. Sci. U. S. A. 79 (1982) 4332–4336.
[6] K. Simons, E. Ikonen, Functional rafts in cell membranes, Nature 387 (1997) 569–572.
[7] G.E. Palade, The fine structure of blood capillaries, J. Appl. Phys. 24 (1953) 1424.
[8] E. Yamada, The fine structure of the gall bladder epithelium of the mouse, J. Biophys. Biochem. Cytol. 1 (1995) 445–458.
[9] R.G. Parton, Caveolae and caveolins, Curr. Opin. Cell Biol. 8 (1996) 542–548.
[10] E.J. Smart, G.A. Graff, M.A. Mcniven, W.C. Sessa, J.A. Engelmann, P.E. Sherer, T. Okamoto, M.P. Lisanti, Caveolins, liquid-ordered domains, and signal transduction, Mol. Cell. Biol. 19 (1999) 7289–7304.
[11] K. Simons, E. Ikonen, Functional rafts in cell membranes, Nature 387 (1997) 569–572.
[12] K. Simons, D. Toomre, Lipid rafts and signal transduction, Mol. Cell. Biol. 1 (2000) 31–41.
[13] D.A. Brown, E. London, Structure and origin of ordered lipid domains on biological membranes, J. Membr. Biol. 164 (1998) 103–114.
[14] T.N. Estep, D.B. Mountcastle, Y. Barenholz, R.L. Biltonen, T.E. Thompson, Thermal behavior of synthetic sphingomyelin–cholesterol dispersions, Biochemistry 18 (1979) 2112–2117.
[15] P.R. Maulik, G.G. Shipley, *N*-palmitoyl sphingomyelin bilayers: structure and interactions with cholesterol and dipalmitoylphosphatidylcholine, Biochemistry 35 (1996) 8025–8034.
[16] S. Veach, S. Keller, Separation of liquid phases in giant vesicles of ternary mixtures of phospholipids and cholesterol, Biophys. J. 85 (2003) 3074–3083.

[17] N. Kahya, D. Scherfeld, K. Bacia, B. Poolman, P. Schwille, Probing lipid mobility of raft-exhibiting model membranes by fluorescence correlation spectroscopy, J. Biol. Chem. 278 (2003) 28109–28115.
[18] J.H. Ipsen, G. Karlstrõm, O.G. Mouritsen, H. Wennerstrõm, M.J. Zuckermann, Phase equilibria in the phosphatidylcholine–cholesterol system, Biochim. Biophys. Acta 905 (1987) 162–172.
[19] S. Arni, S.A. Keilbaugh, A.G. Ostermeyer, D.A. Brown, Association of GAP-43 with detergent-resistant membranes requires two palmitoylated cysteine residues, J. Biol. Chem. 273 (1998) 28478–28485.
[20] S. Munro, Lipid rafts: elusive or illusive? Cell 115 (2003) 377–388.
[21] T.P.W. McMullen, R.N.A.H. Lewis, R.N. McElhaney, Cholesterol–phospholipid interactions, the liquid-ordered phase and lipid rafts in model and biological membranes, Curr. Opin. Colloid Interface Sci. 8 (2004) 459–468.
[22] M.P. Veiga, J.L.R. Arrondo, F.M. Goni, A. Alonso, D. Marsh, Interaction of cholesterol with sphingomyelin in mixed membranes containing phosphatidylcholine, studied by spin-label ESR and IR spectroscopies. A possible stabilization of gel-phase sphingolipid domains by cholesterol, Biochemistry 40 (2001) 2614–2622.
[23] F. Schmidt, Y. Barenholz, T.E. Thompson, A nuclear magnetic resonance study of sphingomyelin in bilayer systems, Biochemistry 16 (1977) 2649–2656.
[24] A. Filippova, B. Munavirova, G. Gröbnerc, M. Rudakovaa, Lateral diffusion in equimolar mixtures of natural sphingomyelins with dioleoylphosphatidylcholine, Magn. Reson. Imaging 30 (2012) 413–421.
[25] C.M. Talbott, I. Vorobyov, D. Borchman, K.G. Taylor, D.B. DuPrè, M.C. Yappert, Conformational studies of sphingolipids by NMR spectroscopy. II. Sphingomyelin, Biochim. Biophys. Acta 939 (1998) 315–326.
[26] P.J. Quinn, C. Wolf, Hydrocarbon chains dominate coupling and phase coexistence in bilayers of natural phosphatidylcholines and sphingomyelins, Biochim. Biophys. Acta 1788 (2009) 1126–1137.
[27] S.A. Pandit, E. Jacobsson, H.L. Scott, Simulation of the early stages of nano-domain formation in mixed bilayers of sphingomyelin, cholesterol, and dioleoylphosphatidylcholine, Biophys. J. 87 (2004) 3312–3322.
[28] T.K.M. Nyholm, M. Nylund, J.P. Slotte, A calorimetric study of binary mixtures of dihydrosphingomyelin and sterols, sphingomyelin or phosphatidylcholine, Biophys. J. 84 (2003) 3138–3146.
[29] B. Ramstedt, P. Leppimaki, M. Axberg, J.P. Slotte, Analysis of natural and synthetic sphingomyelins using high-performance thin-layer chromatography, Eur. J. Biochem. 266 (1999) 997–1002.
[30] M. Kuikka, B. Ramstedt, H. Ohvo-Rekilä, J. Tuuf, J.P. Slotte, Membrane properties of d-*erythro*-*N*-acyl sphingomyelins and their corresponding dihydro species, Biophys. J. 80 (2001) 2327–2337.
[31] C.R. Vieira, J.M. Munoz-Olaya, J. Sot, S. Jimenez-Baranda, N. Izquierdo-Useros, J.L. Abad, B. Apellaniz, R. Delgado, J. Martinez-Picado, A. Alonso, J. Casas, J.L. Nieva, G. Fabrias, S. Manes, F.M. Goni, Dihydrosphingomyelin impairs HIV-1 infection by rigidifying liquid-ordered membrane domains, Chem. Biol. 17 (2010) 766–775.
[32] T. Nyholm, M. Nylund, A. Söderholm, J.P. Slotte, Properties of palmitoyl phosphatidylcholine, sphingomyelin and dihydrosphingomyelin bilayer membranes as reported by different fluorescent reporter molecules, Biophys. J. 84 (2003) 987–997.
[33] S.H. Wu, H.M. McConnell, Phase separations in phospholipid membranes, Biochemistry 14 (1975) 847–854.
[34] J.T. Mason, Mixing behavior of symmetric chain length and mixed chain length phosphatidylcholines in two-component multilamellar bilayers evidence for gel phase and liquid-crystalline phase immiscibility, Biochemistry 27 (1988) 4421–4429.
[35] P.B. Schneider, E.P. Kennedy, Sphingomyelinase in normal human spleens and in spleens from subjects with Niemann–Pick disease, J. Lipid Res. 8 (1967) 202–209.
[36] B.L. Stottrup, S.L. Veach, S.L. Keller, Nonequilibrium behavior in supported lipid membranes containing cholesterol, Biophys. J. 86 (2004) 2942–2954.
[37] M.I. Angelova, D.S. Dimitrov, Liposome electroformation, Faraday Discuss. Chem. Soc. 81 (1986) 303–311.
[38] K.S. Bruzik, M.D. Tsai, A calorimetric study of the thermotropic behavior of pure sphingomyelin diastereomer, Biochemistry 26 (1987) 5364–5368.
[39] M. Kodam, Y. Kawasaki, Structural role of mismatched C–C bonds in a series of d-*erythro*-sphingomyelins as studied by DSC and electron microscopy, Chem. Phys. Lipids 163 (2010) 514–523.
[40] M. Kinoshita, S.A. Goretta, H. Tsuchikawa, N. Matsumori, M. Murata, Characterization of the ordered phase formed by sphingomyelin analogues and cholesterol binary mixtures, Biophysics 4 (2013) 37–49.
[41] S.H. Untracht, G.G. Shipley, Molecular interactions between lecithin and sphingomyelin, J. Biol. Chem. 252 (1977) 4449–4457.
[42] S.L. Veatch, S.L. Keller, Miscibility phase diagrams of giant vesicles containing sphingomyelin, Phys. Rev. Lett. 94 (2005) 148101.
[43] J. Ding, D.Y. Takamoto, A. von Nahmen, M.M. Lipp, K.Y.C. Lee, A.J. Waring, J.A. Zasadzinski, Effects of lung surfactant proteins, SP-B and SP-C, and palmitic acid on monolayer stability, Biophys. J. 80 (2001) 2262–2272.
[44] R.M. Epand, Cholesterol in bilayers of sphingomyelin or dihydrosphingomyelin at concentrations found in ocular lens membranes, Biophys. J. 84 (2003) 3102–3110.
[45] M. Kuikka, B. Ramstedt, H. Ohvo-Rekila, J. Tuuf, J.P. Slotte, Membrane properties of D-*erythro*-N-acyl sphingomyelins and their corresponding dihydro species, Biophys. J. 80 (2001) 2327–2337.
[46] J.M. Seddon, K. Harlos, D. Marsh, Metastability and polymorphism in the gel and fluid bilayer phases of dilauroylphosphatidylethanolamine, J. Biol. Chem. 258 (1983) 3850–3854.
[47] H. Chan, R.M. Epand, The existence of highly ordered phase in fully hydrated dilauroylphosphatidylethanolamine, Biochim. Biophys. Acta 728 (1983) 319–324.
[48] J. Zhao, J. Wu, H. Shao, F. Kong, N. Jain, G. Hunt, G. Feigenson, Phase studies of model biomembranes: macroscopic coexistence of $L_\alpha + L_{\beta'}$, with light-induced coexistence of $L_\alpha + L_o$ phases, Biochim. Biophys. Acta 1487 (2007) 2777–2786.
[49] N.F. Morales-Penningston, J. Wu, E.R. Farkas, S.L. Goh, T.M. Konyakhina, J.Y. Zheng, W.W. Webb, G.W. Feigenson, GUV preparation and imaging: minimizing artifacts, Biochim. Biophys. Acta 1798 (2010) 1324–1332.
[50] J.W. Borst, N.V. Visser, O. Kouptsova, A.J.W.G. Visser, Oxidation of unsaturated phospholipids in membrane bilayer mixtures is accompanied by membrane fluidity changes, Biochim. Biophys. Acta 1487 (2000) 61–73.
[51] C. Dietrich, L.A. Bagatolli, Z.N. Volovyk, N.L. Thompson, M. Levi, K. Jacobson, E. Gratton, Lipid rafts reconstituted in model membranes, Biophys. J. 80 (2001) 1417–1428.
[52] K. Bacia, P. Schwille, T. Kurzchalia, Sterol structure determines the separation of phases and the curvature of the liquid-ordered phase in model membranes, Proc. Natl. Acad. Sci. U. S. A. 102 (2005) 3272–3277.